Thermally Stable Amorphous Mesoporous Aluminophosphates with Controllable P/Al Ratio: Synthesis, Characterization, and Catalytic Performance for Selective O-Methylation of Catechol

Gang Liu, Zhenlü Wang, Mingjun Jia,* Xiujing Zou, Xiaomei Zhu, Wenxiang Zhang,* and Dazhen Jiang

College of Chemistry, Jilin University, Changchun, 130023, China

Received: May 9, 2006; In Final Form: July 13, 2006

Amorphous mesoporous aluminophosphates (AlPO) with P/Al molar ratio in the range 0.8−1.15 are synthesized by using the citric acid (CA) route and are systematically characterized using N_2-adsorption, XRD, SEM, solid-state CP-MAS NMR, FT-IR, TG-DTA, CO_2-TPD, and NH_3-TPD. The characterization studies show that the change in P/Al ratio could affect the structure, texture, thermal stability, and surface acid−base properties of AlPO. Samples with a relatively low P/Al ratio ($\leq$1.0) exhibit uniform amorphous mesoporous character and high thermal stability (up to 1173 K). Partial crystallization of the AlPO framework easily occurred on the sample with higher P/Al ratio ($\geq$1.1), thus leading to significant decrease of surface area and formation of particle pile mesopores. Both weak acid and weak base sites are observed over AlPO materials, and the amounts of acid−base sites can be effectively controlled by adjusting the P/Al ratio. The presence of suitable interaction between citric acid and AlPO framework is critical for the formation of mesoporous structures. Both CA and PO_4 units are considered to be ligands to coordinate with aluminum ions, forming relative uniform complexes (such as CA−Al−PO_4) in the as-synthesized AlPO materials. The mesoporous structure of AlPO materials is obtained after the rapid decomposition of citric acid. Vapor phase selective O-methylation of catechol with methanol reaction is carried out to investigate the catalytic performances of AlPO materials with different P/Al ratios. Among them, $AlP_{1.1}O$ shows the highest activity (88.4% conversion of catechol) and the highest yield of guaiacol (74.3%). The presence of suitable weak acid−base pairs may play an important role on the title reaction.

1. Introduction

The synthesis of mesoporous aluminophosphate materials has received great attention due to its potential applications in catalysis and adsorption.[1−3] Surfactant templating route is a popular way to synthesize lamellar or hexagonal mesoporous AlPO.[4,5] However, one main drawback related to this route is that most of these materials are thermally unstable and therefore collapse upon removal of the surfactants by calcinations.[6−8] Another problem is that it is difficult to obtain porous AlPO with an adjustable P/Al ratio close to or above 1:1 (a usual ratio for microporous aluminophosphates).[5,9−11] Generally, it is well-known that the P/Al molar ratio is a critical parameter for adjusting the acidic−basic property, which can greatly influence the catalytic performance of the aluminophosphate materials.[12,13] Therefore, it is still a rewarding and challenging subject to synthesize stable mesoporous AlPO with a controllable P/Al ratio.

Recently, a few relatively successful examples of thermally stable mesoporous AlPO materials have been reported.[14−19] Cabrera et al.[14] obtained thermally stable (up to 773 K) mesoporous AlPO materials with P/Al ratio in the range of 0.15−0.75 by using long-chain cationic surfactant. Tiemann and Froba[15] synthesized mesoporous AlPO with stoichiometrical composition using single-source precursors $[Al(PO_4)(HCl)(C_2H_5OH)_4]_4$ through alkylamine templating. Zhao and co-workers[16] reported an "acid−base pairs" route for the synthesis of ordered and stable (up to 823 K) mesoporous AlPO material using a block copolymer as template. Lin et al.[17] and our group[18] independently reported the synthesis of thermally stable mesoporous AlPO (up to 1073 K) using preformed precursors of microporous aluminophosphate as inorganic sources. By using this method, a sample with nearly ideal stoichiometry (1.03:1) can be obtained. These progresses demonstrate that the synthesis of thermally stable mesoporous AlPO materials with adjustable P/Al ratio could be realized by pursuing novel approaches.

Different from the general surfactant templating route, Campelo et al.[20] reported that thermally stable amorphous mesoporous aluminophosphate materials can be synthesized by a sol−gel process in the presence of organic additives, such as 1,3-propanediol or 2-methyl-2,4-pentanediol. These materials, though they possess a relatively broad pore size distribution (5 to 50 nm), can keep the mesoporous characteristic even after calcinations at 1073 K. By using a similar strategy, we recently found that amorphous mesoporous aluminophosphates can also be obtained by a nonsurfactant method using citric acid (CA) as organic additive.[21,22] The resulting material exhibits high surface area, narrow pore size distribution, and excellent thermal stability, showing that the citric acid route could be a simple and efficient way to synthesize amorphous mesoporous aluminophosphates with high thermal stability.

In the present work, we attempt to synthesize amorphous mesoporous AlPO with different P/Al molar ratios by using the citric acid route for the purpose to obtain a series of acid−base

* Corresponding authors. Tel: (+86) 431-8499140. Fax: (+86) 431-5168420. Email: jiamj@mail.jlu.edu.cn; zhwenx@mail.jlu.edu.cn.

10.1021/jp062824u CCC: $33.50
Published on Web 08/09/2006

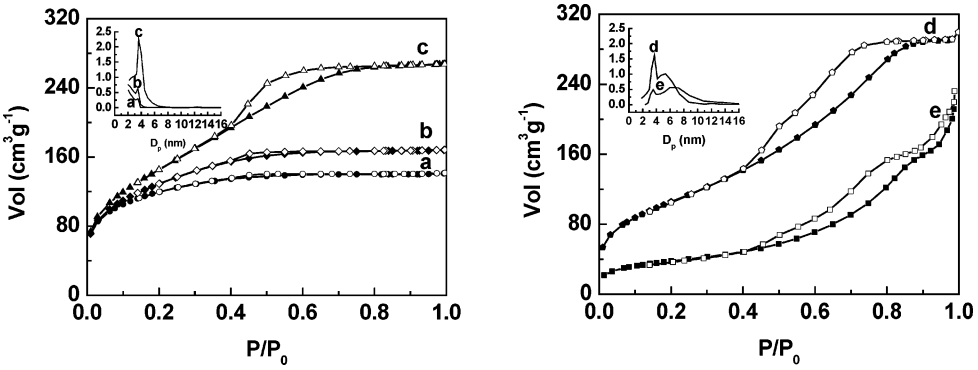

Figure 1. N_2 adsorption−desorption isotherms and BJH pore size distribution (inset) of AlPO calcined at 873 K. (a) $AlP_{0.8}O$, (b) $AlP_{0.9}O$, (c) $AlP_{1.0}O$, (d) $AlP_{1.1}O$, (e) $AlP_{1.15}O$.

bifunctional materials. The effect of the P/Al ratio on the structure, texture, acid−base properties, and thermal stability is investigated by various characterization techniques, including XRD, FT-IR, N_2-adsorption, solid-state CP-MAS NMR spectroscopy, SEM, ICP, DTA, CO_2-TPD, and NH_3-TPD. The formation mechanism of porous structures is also discussed from the viewpoints of the interaction between citric acid and the AlPO framework. Finally, the catalytic performances of mesoporous AlPO with different P/Al ratios are studied for the vapor phase selective O-methylation of catechol.

2. Experimental Section

2.1. Synthetic Procedures. The amorphous mesoporous AlPO materials were synthesized using the following procedure as described previously.[21] Typically, 27 g of CA and 48 g of $Al(NO_3)_3{\cdot}9H_2O$ were dissolved in 200 mL of distilled water, and the resulting solution was stirred at ambient temperature for 30 min. Then a certain amount of H_3PO_4 (85 wt %) was dropped into the solution under vigorous stirring, leading to a composition in molar ratio of 1.0:1.0:*x*:86 $Al(NO_3)_3$/CA/H_3PO_4/H_2O ($x = 0.8, 0.9, 1.0, 1.05, 1.1, 1.15$). Then, a diluted aqueous ammonia (10 wt %) solution was used to adjust the pH value of the solution to 5.0. After standing for 5 h, the mixture was heated at 363 K in open air to remove water and all other volatiles to obtain the as-synthesized precursor. Then the dried solid was calcined at the desired temperature for 3 h to obtain the resulting aluminophosphate materials (denoted as AlP_xO, where *x* means the molar ratio of P/Al). Chemical analysis with ICP reveals that the P/Al molar ratio of calcined AlPO is approximately equal to starting solution.

2.2. Characterization. Powder XRD patterns were recorded on Shimadzu XRD-6000 diffractometer (40 kV, 30 mA) using Ni-filtered *Cu* Kα radiation. N_2 adsorption−desorption isotherms were measured at 77 K, using a Micromeritics ASAP 2010N analyzer. Samples were degassed at 523 K for 8 h before measurements. Specific surface areas were calculated using the BET model. Pore volumes were estimated at a relative pressure of 0.94 (P/P_0), assuming full surface saturation with nitrogen. Pore size distributions were evaluated from desorption branches of nitrogen isotherms using the BJH model. The SEM micrographs were obtained using a Shimadzu SSX-550 microscope. Solid-state ^{27}Al and ^{31}P MAS NMR spectra were carried out on a Varian Infinity plus 400 spectrometer operating at a magnetic field of $B_0 = 9.4$ T with NMR frequencies of 104 MHz for ^{27}Al and 161 MHz for ^{31}P NMR at a spin rate of 10 kHz. FT-IR spectra were recorded on a Nicolet AVATAR 370 DTGS spectrometer (the resolution is 4.0 cm^{-1}). The spectra in the −OH stretching region were obtained following a procedure as described previously.[22] Typically, the dried sample was first pressed into a self-supporting wafer and placed into an infrared cell with CaF_2 windows, then was pretreated at 523 K for 1 h under vacuum conditions prior to IR measurement. DTA experiments were performed using Shimadzu DTG-60 thermal station in flowing air with a heating rate of 10 K·min^{-1}, in the range from room temperature to 1123 K. The aluminum and phosphorus composition analyses were performed via inductively coupled plasma (ICP) on a Perkin Elmer emission spectrometer. Before analysis, 10 mg of AlPO was dissolved in 2 mL of HNO_3 solution (4 mol L^{-1}) at 323 K followed by diluting to 25 mL using distilled water. Temperature-programmed desorption (TPD) was carried out using NH_3 or CO_2 as probe molecules.[23] In a standard procedure, 100 mg of fresh sample was first calcined at 673 K under Ar stream for 60 min, then cooled to 323 K. Ammonia (99.99%) or carbon dioxide (99.95%) was injected into the stream until saturation was reached, and the system was maintained at 323 K for 30 min. After purging the system with flowing Ar for 2 h at 323 K, the sample was heated at the rate of 10 K·min^{-1} in He (30 mL/min), and the concentration change of the desorbed NH_3 or CO_2 was monitored by using an online thermal conductivity detector (TCD).

2.3. Catalytic Tests. The vapor-phase O-methylation of catechol with methanol was carried out in a fixed bed continuous down-flow reactor at atmospheric pressure.[13,23] A quantity of 1.4 g of catalyst (40−60 mesh) was packed in the glass-tube reactor placed in a vertical furnace, and then nitrogen was passed for about 1 h prior to the reaction. The reaction conditions were as follows: catechol/methanol = 1:5 (mole ratio), reaction temperature = 553 K, WHSV = 0.34 h^{-1}. The feed mixture was admitted to the reactor by means of a syringe pump. Evolved gases from the reactor were passed through a condenser and on to a collector that allowed liquids to be withdrawn at required time intervals. The products were analyzed by a gas chromatograph equipped with a capillary column and identified with known standards and GC−MS.

3. Results and Discussion

3.1. Textural and Structural Characterization. The N_2 adsorption isotherms and pore size distributions of various AlPO materials (calcined at 873 K) with different P/Al ratios are shown in Figure 1. As reported previously, the burning of carbon formed by the decomposition of citric acid has been finished at 873 K.[21] Both $AlP_{0.8}O$ and $AlP_{0.9}O$ exhibit irreversible type I + IV isotherms with a small hysteresis loop,[24] implying the co-presence of micropores and mesopores in the low P/Al ratio samples. The sample of $AlP_{1.0}O$ shows a typical type IV isotherm (definition by IUPAC), which is a characteristic of mesoporous materials.[25] The appearance of H2 hysteresis loops

TABLE 1: Selected Synthetic and Physical Data for AlPO Materials Calcined at 873 K

entry	materials	P/Al[a] mol ratio	S_{BET} (m^2/g)	pore vol (cm^3/g)	BJH pore diam[b] (nm)
1	$AlP_{0.8}O$	0.79	427	0.12	2.6
2	$AlP_{0.9}O$	0.91	469	0.19	2.7
3	$AlP_{1.0}O$	1.01	546	0.47	3.4
4	$AlP_{1.05}O$	1.07	428	0.47	4.2
5	$AlP_{1.1}O$	1.13	391	0.49	4.6
6	$AlP_{1.15}O$	1.17	138	0.37	7.4

[a] As measured by ICP chemical analysis. [b] Pore diameters calculated by using the BJH model on the desorption branch of the isotherms.

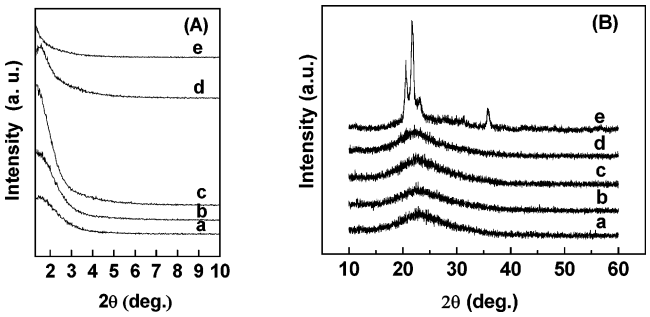

Figure 2. XRD patterns of AlPO calcined at 873 K (A) in the low-angle region (below $2\theta = 10°$) and (B) in the wide-angle region ($10° < 2\theta < 60°$). (a) $AlP_{0.8}O$, (b) $AlP_{0.9}O$, (c) $AlP_{1.0}O$, (d) $AlP_{1.1}O$, (e) $AlP_{1.15}O$.

at relative pressure 0.4−0.8 indicates the presence of "ink-bottle" type pores in this material.[25,26] For the sample of $AlP_{1.1}O$, the sharp inflection of the hysteresis loop shifts toward higher P/P_0, indicating the increment of pore size. This can be further verified by Barret−Joyner−Halenda (BJH) calculations; that is, the mean pore size of $AlP_{1.0}O$ is determined to be 3.4 nm, whereas $AlP_{1.1}O$ possesses two types of pore size distribution centered at 3.6 and 5.4 nm, respectively. As for the $AlP_{1.15}O$ sample, an isotherm with a hysteresis loop at relative pressure 0.40−0.99 is observed, corresponding to relatively large pore size (ca. 7.4 nm, Table 1) and broad pore size distributions (2−11 nm). Generally, the hysteresis loop in the partial pressure region of 0.4−0.8 can be associated with framework mesoporosity, whereas the hysteresis loop at high partial pressure ($p/p_0 > 0.8$) is indicative of textural mesoporosity arisen from voids between the particles.[27,28]

Table 1 shows the textural properties of various AlPO materials calcined at 873 K. It is seen that the samples with P/Al ratio from 0.8 to 1.1 possess relatively high surface areas. Among them, $AlP_{1.0}O$ exhibits the highest surface area (546 $m^2\ g^{-1}$). The pore volume and the average pore size increased from 0.12 $cm^3\ g^{-1}$/2.6 nm to 0.49 $cm^3\ g^{-1}$/4.6 nm with P/Al changing from 0.8 to 1.1. With the further increase of P/Al ratio to 1.15, the surface area and the pore volume decrease considerably to 138 $m^2\ g^{-1}$ and 0.37 $cm^3\ g^{-1}$, respectively.

The X-ray powder diffraction patterns of the sample with different P/Al molar ratio (calcined at 873 K) are shown in Figure 2. Analysis for all samples shows that only very weak and broad reflections (or even negligible for the $AlP_{1.15}O$ sample) can be observed in low-angle range (Figure 2A), indicating the absence of long-range order in these AlPO materials. In the wide-angle region ($10° < 2\theta < 60°$), samples with P/Al ratio from 0.8 to 1.1 exhibit only one very broad band in the 2θ range from 15° to 30°, which is a characteristic of amorphous aluminophosphates.[20,29] A few weak diffraction peaks appear on the pattern of $AlP_{1.15}O$ material, which can be assigned to the presence of two types of crystallization phases of tridymite ($2\theta = 20.4$, 21.6, 23.2) and α-cristobalite ($2\theta = 35.8$).[20]

Figure 3 shows the SEM images of $AlP_{0.9}O$, $AlP_{1.0}O$, and $AlP_{1.1}O$ (calcined at 873 K). Samples $AlP_{0.9}O$ and $AlP_{1.0}O$ exhibit a quite uniform filmlike shape, whereas a little particle agglomeration is observed on the relative coarse surface of $AlP_{1.1}O$. Combined with the characterization results of N_2-adsorption and XRD, we may speculate that the occurrence of particle agglomeration should be related to the partial crystallization of AlPO framework on the sample with relatively high P/Al ratios (≥1.1), thus leading to significant decrease of surface area and formation of particle pile mesopores.

The ^{27}Al MAS NMR spectra of AlPO (calcined at 873 K) are measured to obtain the information on the coordination environment of aluminum. As shown in Figure 4, the peak at 36 ppm is assigned to tetrahedral $Al(OP)_4$ groups, and the signals at −13 ppm can be attributed to octahedrally coordinated Al species (i.e., $Al(OP)_x(OH)_{6-x}$).[7,8,21,30] In the case of $AlP_{0.9}O$ and $AlP_{1.0}O$, both tetrahedrally and octahedrally coordinated Al signals are observed, indicating the co-presence of AlO_4 and AlO_6 species. For the $AlP_{1.1}O$ sample, no detectable signals assigned to octahedrally coordinated Al species could be observed, indicating that almost all Al atoms link with O−P to form $Al(OP)_4$ groups. The slight excess of P species (in comparison with the sample of $AlP_{1.0}O$) can make all Al species form tetrahedral $Al(OP)_4$ groups, thus resulting in the disappearance of the signal of octahedrally coordinated Al species. For the $AlP_{1.15}O$ sample, the narrowing of the resonance pattern as well as the appearance of the signal of octahedrally coordinated Al species suggest that the coordination environment of Al species has changed, which should be mainly caused by the partial crystallization of this material.

The ^{31}P MAS NMR spectra of various AlPO samples (calcined at 873 K) are shown in Figure 5. All the samples exhibit strong signal in the chemical shift range −25 to −30 ppm, which can be mainly attributed to the P atom in tetrahedral coordination with O−Al bands, as the $P(OAl)_4$ unit.[7,8,21,30] The relatively broad resonance may imply the presence of a small amount of phosphorus species, which coordinated partly with H_2O or OH groups (i.e., $P(OAl)_x(HO)_{4-x}$).[7,8] Compared with the three samples of $AlP_{0.9}O$, $AlP_{1.0}O$, and $AlP_{1.1}O$, the signal of $AlP_{1.15}O$ shifts to high field and splits into two shoulder peaks (−27.8 and −29.3 ppm). According to the XRD results, the change of coordination environments of the P atom in $AlP_{1.15}O$ can be mainly assigned to the appearance of a certain amount of mixed crystallization phases of tridymite and α-cristobalite.

FT-IR spectra of AlPO samples (calcined at 873 K) in the −OH stretching region are measured (Figure 6). The sharp band at 3670 cm^{-1} is assigned to the nonbonded surface P−OH groups.[20] A very broad band around 3540 cm^{-1} can be assigned to surface hydroxyl groups, most likely phosphorus ones, perturbed by a hydrogen bridge bond from a surface hydroxyl band.[20] As shown in Figure 6, the bands at 3670 and 3540 cm^{-1} increase in intensity with the increment of P/Al ratio from 0.9 to 1.1. For the sample of $AlP_{1.15}O$, only a very weak signal at 3670 cm^{-1} is observed, indicating that the condensation of surface P−OH groups is nearly completed in the sample with high P/Al ratio (i.e., above 1.15). These results suggest that the amounts of surface P−OH significantly correlate with the P/Al composition of AlPO materials. As confirmed by the characterization results of XRD and NMR, we knew that the partial crystallization had occurred on the sample of $AlP_{1.15}O$. Therefore, it is very reasonable to see the obvious decrease of the

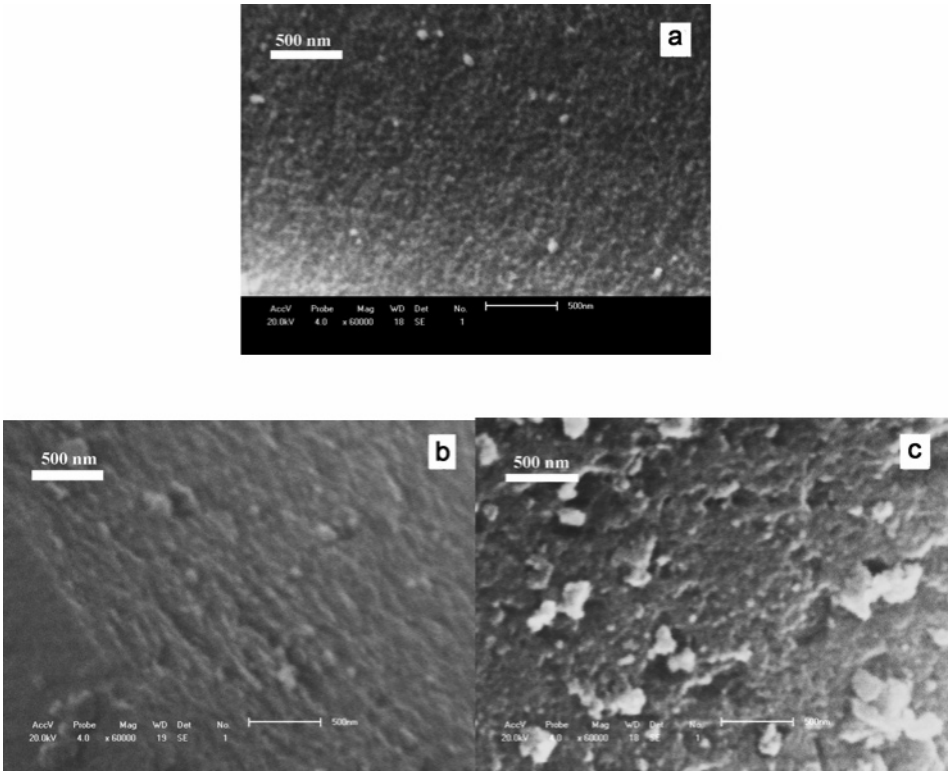

Figure 3. SEM images of AlPO calcined at 873 K. (a) $AlP_{0.9}O$, (b) $AlP_{1.0}O$, (c) $AlP_{1.1}O$.

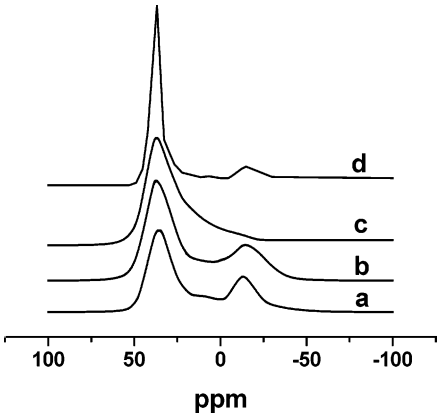

Figure 4. Solid-state ^{27}Al MAS NMR spectra of AlPO calcined at 873 K. (a) $AlP_{0.9}O$, (b) $AlP_{1.0}O$, (c) $AlP_{1.1}O$, (d) $AlP_{1.15}O$.

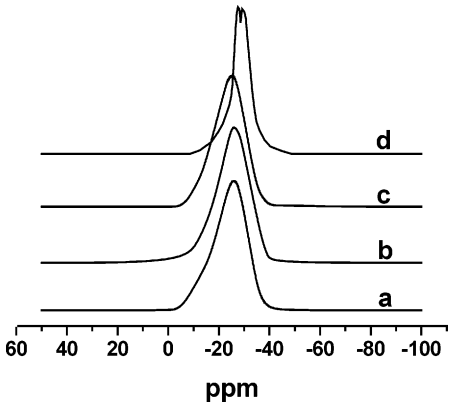

Figure 5. Solid-state ^{31}P MAS NMR spectra of AlPO calcined at 873 K. (a) $AlP_{0.9}O$, (b) $AlP_{1.0}O$, (c) $AlP_{1.1}O$, (d) $AlP_{1.15}O$.

surface P−OH groups on $AlP_{1.15}O$ as shown in the IR spectrum of this sample.

The acidity and basicity of various AlPO materials with different P/Al ratios are determined by means of CO_2-TPD and NH_3-TPD (Figure 7). The CO_2-TPD profiles show that all tested samples have a broad desorption peak at low temperatures (in range of 390−413 K), indicating the presence of weak basic sites. With the increase of the P/Al ratio, the desorption peak of CO_2 shifts slightly toward low temperature, indicating that the relative strength of the basic sites decreases somewhat with the increase of P content. Meanwhile, the area of desorption peak also decreases with the increase of the P/Al ratio, which refers to the decrease of basic amount.

NH_3-TPD profiles of various samples are presented in Figure 7B. All the samples show one broad NH_3 desorption peak centered about 430 K, indicating the existence of weak acid sites with identical acid strength.[31] The acidic amount increases with P/Al ratio and reaches maximum when the P/Al ratio is 1.1. By further increasing the P/Al ratio to 1.15, the acid amount decreases dramatically, which should be mainly caused by the partial crystallization of this material.

These characterization results show that the synthesis of amorphous mesoporous aluminophosphates by using the citric acid route could be achieved successfully in the P/Al ratio range of 0.8−1.15. The P/Al composition has an important effect on the structure, texture, and acid−base properties of these AlPO materials. By varying P/Al ratio, the amount of acid−base sites can be effectively adjusted. Combining the results of NH_3-TPD with FT-IR, it can be seen that there is a direct relation between the acid amount (TPD results) and the number of P−OH sites (FT-IR results). Both the area of NH_3 desorption peak and the intensity of P−OH signal increase with P/Al ratio from 0.9 to 1.1, but decrease with further increase of P/Al ratio to 1.15. Therefore, it seems that the P−OH groups should be the main source of acid sites on the surface of AlPO materials.

3.2. Investigation of Thermal Stabilities. To investigate the effect of P/Al on the thermal stability of mesoporous AlPO, samples $AlP_{0.9}O$, $AlP_{1.0}O$, and $AlP_{1.1}O$ as representative materi-

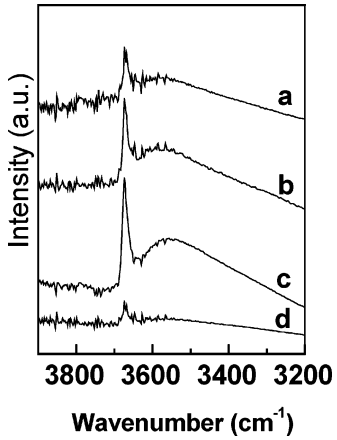

Figure 6. FT-IR spectra in the hydroxyl region of AlPO calcined at 873 K. (a) $AlP_{0.9}O$, (b) $AlP_{1.0}O$, (c) $AlP_{1.1}O$, (d) $AlP_{1.15}O$.

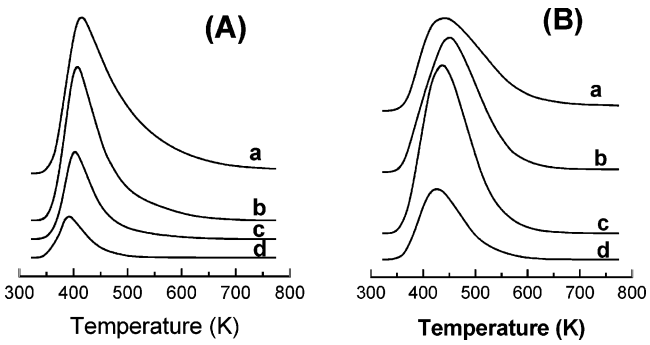

Figure 7. CO_2-TPD (A) and NH_3-TPD (B) patterns of AlPO calcined at 873 K. (a) $AlP_{0.9}O$, (b) $AlP_{1.0}O$, (c) $AlP_{1.1}O$, (d) $AlP_{1.15}O$.

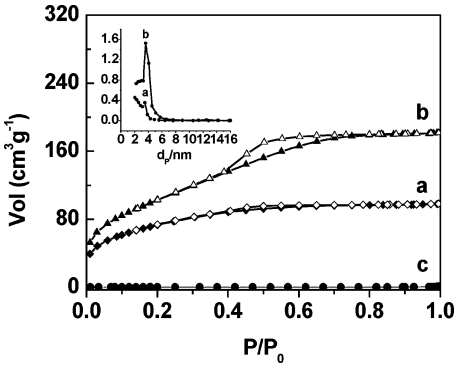

Figure 8. N_2 adsorption−desorption isotherms and BJH pore size distribution (inset) of AlPO calcined at 1173 K. (a) $AlP_{0.9}O$, (b) $AlP_{1.0}O$, (c) $AlP_{1.1}O$.

als are calcined at 1173 K for 3 h. As shown in Figure 8, $AlP_{0.9}O$ and $AlP_{1.0}O$ calcined at 1173 K exhibit types of isotherms and narrow pore size distributions similar to those of the corresponded samples calcined at 873 K (Figure 1). Increasing the calcined temperatures just leads to the decrease of the surface area and pore volume (see Table 2). XRD patterns show that both $AlP_{0.9}O$ and $AlP_{1.0}O$ still maintain the amorphous structure (Figure 9). These results suggest that the mesoporous structure of these two samples is stable at such high temperatures. As for the $AlP_{1.1}O$ sample (calcined at 1173 K), the total adsorption volume is very low, and the surface area and pore volume decrease dramatically to very low level, indicating that the mesoporous structure collapsed at this temperature. The XRD pattern shows that the mixture crystalline phase of tridymite and α-cristobalite with high crystallization formed after the calcination of $AlP_{1.1}O$ at 1173 K (Figure 9). Further study shows that the amorphous mesoporous structure of $AlP_{1.1}O$ could maintain up to 973 K (Figure 9 and Table 2). To our knowledge, this is the highest thermal stable temperature ever reported for the mesoporous aluminophosphates with such a P/Al ratio. These results suggest that the citric acid route can offer a unique advantage for creating the thermal stable amphorous mesoporous AlPO materials with different P/Al ratios.

TABLE 2: Textural Properties of AlPO Materials Calcined at Different Temperatures

entry	materials	calcination temp (K)	S_{BET} (m^2/g)	pore vol (cm^3/g)	BJH pore diam[a] (nm)
1	$AlP_{0.9}O$	1173	268	0.12	2.7
2	$AlP_{1.0}O$	1173	379	0.33	3.7
3	$AlP_{1.1}O$	1173	1.9	0.003	10.9
4	$AlP_{1.1}O$	973	280	0.36	3.9
5	$AlP_{1.1}O$	1023	194	0.25	4.1
6	$AlP_{1.1}O$	1073	34	0.05	4.9

[a] Pore diameters calculated by using the BJH model on the desorption branch of the isotherms.

3.3. Discussion. Some additional characterizations are carried out to study the formation mechanism of the porous structures of AlPO materials. Figure 10 shows the DTA profiles of pure citric acid and as-synthesized precursors of $AlP_{0.9}O$, $AlP_{1.0}O$, and $AlP_{1.1}O$. For the sample of pure citric acid, three main endothermic peaks at 329, 427, and 483 K are observed, which can be ascribed to the elimination of water of crystallization, the melting of the citric acid crystal, and the decomposition of citric acid, respectively.[26] The strong exothermic peak around 778 K can be attributed to the burning of carbon formed by the decomposition of citric acid.[21]

For the three as-synthesized precursors of AlPO materials, the endothermic peaks corresponding to the elimination of water of citric acid crystallization and the melt of citric acid crystal are nearly undetectable. The disappearance of endothermic peaks corresponding to the melt of citric acid suggests that citric acid could interact with aluminum ions, forming a relative uniform complex in the as-synthesized AlPO materials.[22] The endothermic peak corresponded to the decomposition of citric acid shifts slightly toward higher temperatures in comparison with that of pure citric acid, which may also suggest the existence of a weak interaction between citric acid and the AlPO network. The appearance of a very strong exothermic peak at ca. 530 K should be mainly caused by the decomposition of some nitrates, such as ammonium nitrates.[21] Notably, the exothermic peak of nitrates decomposition and the endothermic peak of burning of carbon shift somewhat to higher temperatures with the increase of the P/Al ratio, suggesting that the intensity of the interaction between citric acid and the AlPO network may be varied with the change of the P/Al ratio.

Figure 11 shows the FT-IR spectra of $AlP_{1.0}O$ at various heating temperatures. The peaks at 1110 and 468 cm^{-1} can be assigned to triply degenerate P−O stretching vibration and triply degenerate O−P−O bending vibration of tetrahedral PO_4^{3-}, respectively.[20,32] The intensity of these two peaks increases considerably with heating temperatures. The signal at 695 cm^{-1}, which is the characteristic stretching vibration of Al−O in combination with P−O,[20] begins to appear after the sample is heated at 573 K and becomes significant with increasing temperature. Considering the fact that citric acid is decomposed in the range 473−573 K, we can speculate that the formation of the Al−O−P framework mainly occurred concomitantly with the decomposition of citric acid.

The ^{27}Al MAS NMR spectrum of the as-synthesized $AlP_{1.0}O$ shows one peak centered at −3.2 ppm, which can be assigned to the six-coordinated Al species (Figure 12A).[10,11,33] The

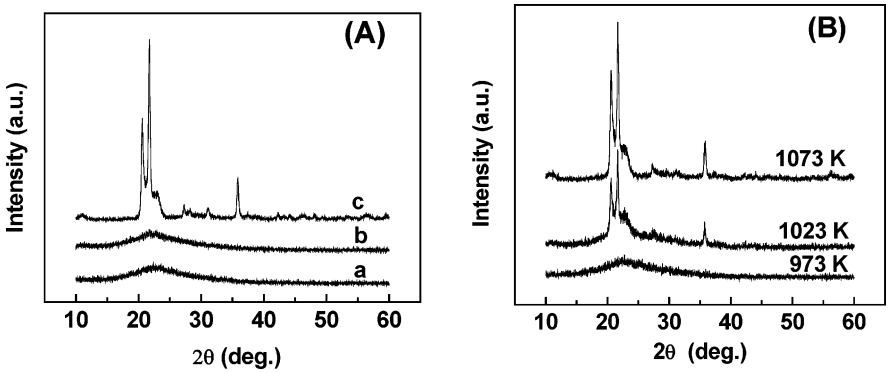

Figure 9. XRD patterns of (A) AlPO calcined at 1173 K. (a) $AlP_{0.9}O$, (b) $AlP_{1.0}O$, (c) $AlP_{1.1}O$. (B) $AlP_{1.1}O$ calcined at different temperatures.

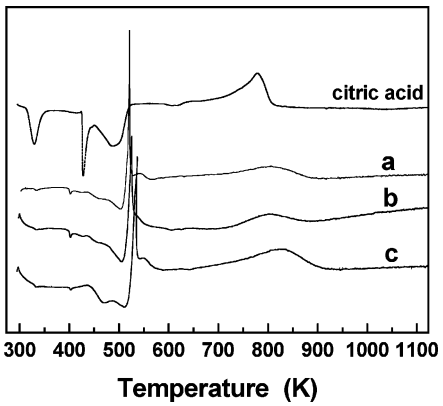

Figure 10. DTA profiles of pure citric acid and as-synthesized precursors of AlPO. (a) $AlP_{0.9}O$, (b) $AlP_{1.0}O$, (c) $AlP_{1.1}O$.

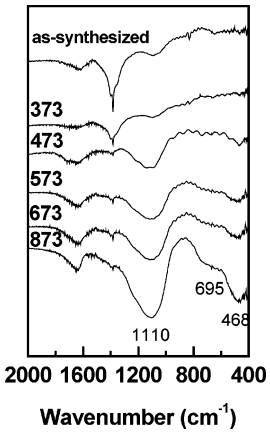

Figure 11. FT-IR spectra of $AlP_{1.0}O$ at various heating temperatures. Numbers on the spectra indicate heating temperature (K).

absence of tetrahedrally coordinated Al species indicates that the condensation reaction of Al and P species to form the framework of mesoporous APO did not occur at this stage. This point can be further confirmed by the ^{31}P MAS NMR spectrum of the as-synthesized $AlP_{1.0}O$ (Figure 12B), since no detectable signal of $P(OAl)_4$ unit (generally in the range -19 to -30 ppm) can be observed in the spectrum.[11] The appearance of several strong signals at -7.3, -11.2, and -16.8 ppm suggests that the coordination environment of P species is rather complicated in the as-synthesized $AlP_{1.0}O$ sample. It has been reported that the chemical shift of ^{31}P species can be influenced by several factors, including the number of surrounding aluminums and the nature of the ligands in the second coordination sphere of phosphorus.[11,34] Generally, the ^{31}P signals with relatively low-field chemical shifts (0 to -13 ppm) can be assigned to the P species with very low degree of condensation or chain-end phosphorus groups.[10,35,36] Therefore, for our as-synthesized $AlP_{1.0}O$ sample, we may assign the three chemical shifts at -7.3, -11.2, and -16.8 ppm to the P species with 1−3 six-coordinated Al species. As noted previously, no gelation or precipitation occurred in the preparation process, which is quite different from the general sol−gel and/or precipitation routes in the presence of organic additives for getting mesoporous materials.[21] To our knowledge, citric acid can bind with Al^{3+} to form a relatively stable complex in aqueous solution,[37] thus inhibiting the hydrolysis and condensation reaction of Al and P species to form a solid AlPO network. On the basis of these results and the related literature, we can conclude here that both CA and PO_4 units can function as ligands to coordinate with aluminum ions, thus forming relative uniform complexes (such as CA−Al−PO_4) in the as-synthesized AlPO materials.

Combined with other characterization results, we have known that the Al−O−P framework is formed gradually by condensation reaction of P and Al species with the increase of heating temperatures. The mesoporous structure of AlPO materials is obtained after the rapid decomposition of citric acid. This formation process is quite different from that of the general surfactant templating route, in which the condensation reaction of P and Al species has been nearly completed (at least to very high level) on the surface of surfactant assemblies after the hydrothermal treatment.[10,11] Additionally, it has been reported that the synthesis of mesoporous AlPO materials under the required alkaline conditions of surfactant system always leads to a P/Al ratio less than 1, which is mainly because the alkaline conditions favor the complete condensation of the Al species rather than P species.[11,19]

In our case, the unique pore formation process of AlPO materials in the presence of citric acid can provide an opportunity to control the P/Al composition of the resulting AlPO materials. Thus, amorphous mesoporous AlPO materials with a relatively high P/Al ratio (e.g., $AlP_{1.1}O$) can be obtained. The presence of uniform complexes (containing citric acid, P, and Al species), as well as a suitable interaction between citric acid and Al species, should be critical for the formation of uniform and thermal stable mesoporous AlPO material. The reason for the relatively low thermal stability of the sample with high P/Al ratio might be because a restructured reaction easily occurred on the P-rich materials, as suggested by Kimura.[38]

3.4. Catalytic Performances. The catalytic performance of amorphous mesoporous AlPO materials are investigated for vapor phase selective O-methylation of catechol with methanol, which is an acid and/or base catalytic reaction for the production of guaiacol (an important intermediate in the production of fine chemicals).[13,23] Previously, it has been found that amorphous aluminophosphates, prepared by conventional precipitation method, are active catalysts for the title reaction.[13] The catalytic

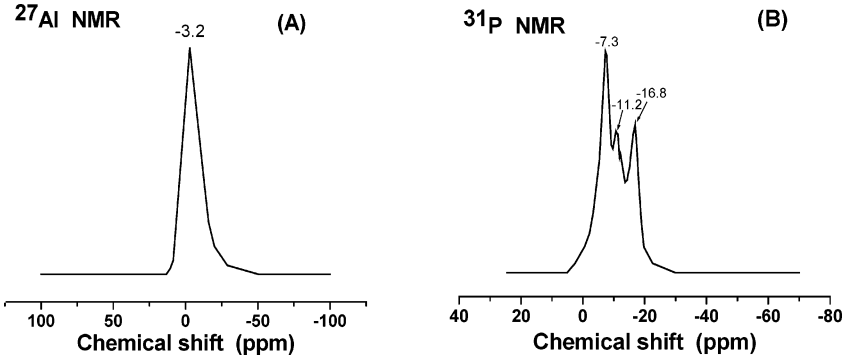

Figure 12. Solid-state MAS NMR spectra of as-synthesized sample $AlP_{1.0}O$.

TABLE 3: Results of Catalytic O-Methylation of Catechol Using Various AlPO Materials Calcined at 873 K

	conversion of	selectivit y (%)			yield (%)		
catalysts	catechol (%)	guaiacol	veratrole	others[b]	guaiacol	veratrole	others[b]
$AlP_{0.9}O$	44.6	66.3	3.1	30.6	29.6	1.4	13.6
$AlP_{1.0}O$	74.3	56.7	4.9	38.4	42.1	3.6	28.5
$AlP_{1.05}O$	84.1	68.3	6.9	24.8	57.4	5.8	20.9
$AlP_{1.1}O$	88.4	84.1	9.5	6.4	74.3	8.4	5.7
$AlP_{1.15}O$	65.2	88.6	4.7	6.7	57.8	3.1	4.4

[a] Reaction conditions: $m_{cat} = 1.4$ g; catechol/methanol = 1/5 mol; WHSV = 0.34 h^{-1}; reaction temp = 553 K; reaction time = 3 to 4 h. [b] Other side products include mainly 3-methylcatechol, 4-methylcatechol, 2-methoxy-4- methylphenol, and so forth.

activity and selectivity of these catalysts can be considerably influenced by the change of the P/Al ratio.

Table 3 shows the catalytic data of the mesoporous AlPO materials with different P/Al ratios (calcined at 873 K). All the samples exhibit good activity under tested conditions. The conversion of catechol increases continuously with the increment of the P/Al ratio and reaches a maximum of 88.4% catechol conversion when the P/Al ratio is 1.1. Then the reaction activity decreases obviously with further increase in the P/Al ratio. The selectivity of guaiacol is varied with the change of the P/Al ratio, and relatively high selectivity can be obtained on the samples with high P/Al ratio (i.e., $AlP_{1.1}O$ and $AlP_{1.15}O$). Among them, $AlP_{1.1}O$ shows the highest activity (88.4% conversion of catechol) and the highest yield of guaiacol (74.3%), which is much higher than those of amorphous aluminophosphates prepared by conventional precipitation method.[13] These results suggest that the catalytic performances for the vapor-phase O-methylation of catechol with methanol can be considerably improved by adjusting the P/Al ratio of the mesoporous AlPO materials.

The CO_2-TPD and NH_3-TPD results have shown that all AlPO materials with different P/Al ratios possess weak acid−base bifunction properties. Both the acidic and basic amounts of the samples are variable with the change in the P/Al ratio. Comparing the acidic−basic characterization results with the catalytic reaction data, we found that the sample of $AlP_{1.1}O$, which contains the largest amount of acid sites and relatively small amount of base sites, exhibits the highest conversion of catechol (88.4%) and the highest selectivity of guaiacol (84.1%). The two samples of $AlP_{0.9}O$ and $Al_{1.0}PO$, which contain relatively low amounts of weak acid sites and high amounts of weak base sites, show relatively low activity and poor selectivity to guaiacol. The $AlP_{1.15}O$ sample containing the lowest amount of basic sites exhibits the highest selectivity of guaiacol. These results suggest that there should be a direct relationship between the weak acid amount and the catalytic activities for the methylation of catechol, and the existence of a high amount of weak basic sites might be responsible for the decrease of guaiacol selectivity.

Previously, Vishwanathan et al.[39] proposed that the presence of weak basic sites on the catalyst are primarily important for the formation of mono O-methylated product (guaiacol) by the study of a few types of solid-base catalysts. In our recent work, we found that the presence of strong acidic and/or basic sites favors the formation of C-methylated products, and the weak acidic−basic characteristics of the Ti-containing aluminum phosphate catalysts should be responsible for the high selectivity to mono O-methylation product (guaiacol).[23,40] Combining these related literature reports and the results in this work, we may conclude that there should be some synergic interaction between the acid sites and the base sites for the activation of the reactants, or we can say that the presence of suitable weak acid−base pairs may play a critical role on the title reaction.

4. Conclusion

Amorphous mesoporous aluminophosphates with different P/Al molar ratios in the range 0.8−1.15 have been synthesized by using the citric acid route. The P/Al ratio can affect the structure, texture, thermal stability, as well as surface acid−base properties of AlPO. Both weak acid and weak base sites are observed over AlPO materials, and the amounts of acid−base sites can be effectively controlled by adjusting the P/Al ratio. Citric acid and PO_4 units can function as ligands to coordinate with aluminum ions, forming relative uniform complexes in the as-synthesized AlPO materials. The mesoporous structure of AlPO materials is obtained after the rapid decomposition of citric acid. This unique pore formation process plays an important role in controlling the P/Al composition of the final AlPO materials. The catalytic performances for the vapor-phase O-methylation of catechol with methanol can be considerably improved by adjusting the P/Al ratio of the mesoporous AlPO materials, and there should be some synergic interaction between the acid sites and the base sites for the activation of the reactants.

Acknowledgment. This work is supported by the Development Project of Science and Technology of Jilin Province (No. 20040563), the Specialized Research Fund for the Doctoral Program of Higher Education (20040183003), CNPC (JTGS 20040010), the National Natural Science Foundation of China

(No. 20403006), and the State Basic Research Project (973 Program, No. 2005CB221405).

References and Notes

(1) Lu, J.; Ranjit, K. T.; Rungrojchaipan, P.; Kevan, L. *J. Phys. Chem. B* **2005**, *109*, 9284.
(2) Selvam, P.; Mohapatra, S. K. *J. Catal.* **2006**, *238*, 88.
(3) Kimura, T. *Chem. Mater.* **2005**, *17*, 337.
(4) Tiemann, M.; Froba, M. *Chem. Mater.* **2001**, *13*, 3211.
(5) Kimura, T. *Microporous Mesoporous Mater.* **2005**, *77*, 97.
(6) Schuth, F. *Chem. Mater.* **2001**, *13*, 3184.
(7) Tiemann, M.; Schulz, M.; Jager, C.; Froba, M. *Chem. Mater*. **2001**, *13*, 2885.
(8) Wang, L.; Tian, B.; Jie, F.; Liu, X.; Yong, H.; Yu, C.; Tu, B.; Zhao, D. *Microporous Mesoporous Mater.* **2004**, *67*, 123.
(9) El Haskouri, J.; Guillem, C.; Latorre, J.; Beltran, A.; Beltran, D.; Amoros, P. *Chem. Mater.* **2004**, *16*, 4359.
(10) Khimyak, Y. Z.; Klinowski, J. *Phys. Chem. Chem. Phys.* **2000**, *2*, 5275.
(11) Luan, Z.; Zhao, D.; He, H.; Klinowski, J.; Kevan, L. *J. Phys. Chem. B* **1998**, *102*, 1250.
(12) Bautista, F. M.; Campelo, J. M.; Luan, G. D.; Marinas, J. M.; Quiros, R. A.; Romero, A. A. *Appl. Catal., A* **2003**, *243*, 93.
(13) Li, X.; Zhang, W.; Liu, G.; Jiang, L.; Zhu, X.; Pan, C.; Jiang, D.; Tang, A. *React. Kinet. Catal. Lett.* **2003**, *79*, 365.
(14) Cabrera, S.; Haskouri, J. E.; Guillem, C.; Beltran-Porter, A.; Beltran-Porter, D.; Mendioroz, S.; Marcos, M. D.; Amoros, P. *Chem. Commun.* **1999**, 333.
(15) Tiemann, M.; Froba, M. *Chem. Commun.* **2002**, 406.
(16) Tian, B.; Liu, X.; Tu, B.; Yu, C.; Jie, F.; Wang, L.; Xie, S.; Stucky, G. D.; Zhao, D. *Nat. Mater.* **2003**, *2*, 159.
(17) Lin, K.; Wang, L.; Sun, Z.; Yang, Q.; Di, Y.; Zhang, D.; Jiang, D.; Xiao, F. *Chem. Lett.* **2005**, *34*, 516.
(18) Zhou, Z.; Liu, G.; Zhang, W.; Liao, X.; Hou, Y.; Jia, M. *Mater. Lett.* **2005**, *59*, 3503.
(19) Ho, L.; Yukushima, S.; Morikawa, R.; Asaka, N.; Nishiguchi, H.; Nagaoka, K.; Takita, Y. *Colloids Surf., A* **2005**, *268*, 40.
(20) Campelo, J. M.; Jaraba, M.; Luna, D.; Luque, R.; Marinas, J. M.; Romero, A. A. *Chem. Mater.* **2003**, *15*, 3352.
(21) Liu, G.; Jia, M.; Zhou, Z.; Zhang, W.; Wu, T.; Jiang, D. *Chem. Commun.* **2004**, 1660.
(22) Liu, G.; Jia, M.; Zhou, Z.; Wang, L.; Zhang, W.; Jiang, *D. J. Colloid Interface Sci.* **2006**, YJCIS12317.
(23) Zhu, X.; Jia, M.; Li, X.; Liu, G.; Zhang, W.; Jiang, D. *Appl. Catal., A* **2005**, *282*, 155.
(24) Carati, A.; Ferraris, G.; Guidotti, M.; Moretti, G.; Psaro, R.; Rizzo, C. *Catal. Today* **2003**, *77*, 315.
(25) Sing, K. S. W.; Everett, D. H.; Haul, R. A. W.; Moscou, L.; Pierotti, R. A.; Rouquerol, J.; Siemieniewska, T. *Pure Appl. Chem.* **1985**, *57*, 603.
(26) Takahashi, R.; Sato, S.; Sodesawa, T.; Kawakita, M.; Ogura, K. *J. Phys. Chem. B* **2000**, *104*, 12184.
(27) Tanev, P. T.; Pinnavaia, T. *J. Chem. Mater.* **1996**, *8*, 2068.
(28) Brutchey, R. L.; Goldberger, J. E.; Koffas, T. S.; Tilley, T. D. *Chem. Mater.* **2003**, *15*, 1040.
(29) Bautista, F. M.; Campelo, J. M.; Garcia, A.; Luan, D.; Marinas, J. M.; Romero, A. A.; Colon, G.; Navio, J. A.; Macias, M. *J. Catal.* **1998**, *179*, 483.
(30) Zhao, D.; Luan, Z.; Kevan, L. *Chem. Commun.* **1997**, 1009.
(31) Zhao, J.; Tian, B.; Yue, Y.; Hua, W.; Zhao, D.; Gao, Z. *J. Mol. Catal. A: Chem.* **2005**, *242*, 218.
(32) Mtalsi, K.; Jei, T.; Montes, M.; Tayane, S. *J. Chem. Technol. Biotechnol.* **2001**, *76*, 128.
(33) Kimura, T.; Sugahara, Y.; Kuroda, K. *Chem. Mater.* **1999**, *11*, 508.
(34) Sayari, A.; Moudrakovski, I. L.; Reddy, J. S. *Chem. Mater.* **1996**, *8*, 2080.
(35) Zhang, L.; Eckert, H. *Solid State Nucl. Magn. Reson.* **2004**, *26*, 132.
(36) Waki, H.; Hatano, M. *Polyhedron* **1982**, *1*, 69.
(37) Motekaitis, R. J.; Martell, A. E. *Inorg. Chem.* **1984**, *23*, 18.
(38) Kimura, T. *Chem. Mater.* **2005**, *17*, 5521.
(39) Vishwanathan, V.; Ndou, S.; Sikhwivhilu, L.; Plint, N.; Raghavan, K. V.; Coville, N. J. *Chem. Commun.* **2001**, 893.
(40) Liu, G.; Li, X.; Zhu, X.; Jia, M.; Wu, S.; Zhang, W.; Jiang, D. *Chem. J. Chin. Univ.* **2005**, *26*, 1492.